

# Numerical Study on Compressive Concrete as a Strain Softening Material

Wataru KURAMOTO\*, Hiroaki KITO<sup>H</sup>\*\* and Hajime OHUCHI<sup>H</sup>\*\*\*

(Received September 30, 2009)

## Synopsis

The prediction of post peak behavior of compressive concrete is significant especially for ductility based on seismic design of reinforced concrete members. The present paper describes numerical modeling of post peak behavior of compressive concrete as a strain softening material with constitutive law based on incremental elasto plastic theory formulated in a strain space. A series of numerical parametric studies have been conducted for the existing experimental results of compressive concrete including useful post peak behavior test.

**KEY WORDS:** Post-Peak Behavior, Compressive Concrete, Strain-Softening, Strain Space Formulation

## 1. Introduction

It is significant to predict plastic deformation capacity of reinforced concrete members, i.e. how compressive concrete can deform and also how it can sustain further compressive stress. Post peak behavior of compressive concrete is deeply related to existence of confinement stress due to lateral reinforcement.

As illustrated in Fig.1, typical stress strain relationship under uniaxial compression, unconfined concrete provides steep descending branch. However, the slope of that branch can be improved milder shown as the dotted line, once effective lateral confinement is provided so that volumetric expansion is restricted by lateral reinforcement such as hoops or ties. Appropriate numerical modeling for such phenomena can be effective to predict rigorously the post peak behavior of reinforced concrete members.

The present study investigates nonlinear constitutive model based on incremental plastic theory with a loading function defined in strain space, proposed by Mizuno and Hatanaka<sup>1)</sup>.

The purpose of the study is to verify effectiveness of the model through numerical finite element simulations for several existing experimental results with strain softening behavior.

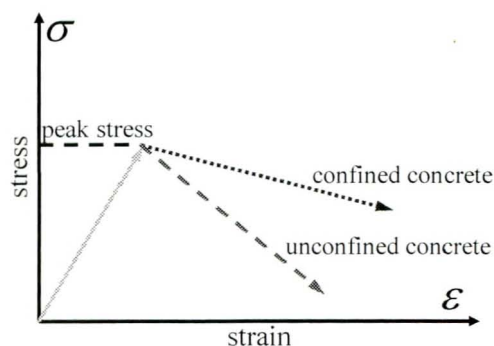


Fig.1 Stress-strain relation of concrete under uniaxial compression

\* Student, Master Course of Dept. of Civil Engineering

\*\* Associate Professor, Dept. of Civil Engineering

\*\*\* Professor, Dept. of Civil Engineering

## 2. Existing Experiments on Strain Softening of Compressive Concrete

There are many experimental studies on the strain softening behavior of compressive concrete with various lateral pressures, those inform us their stress strain relations and also failure envelopes in various combination of stress states. Form the viewpoint of existence of lateral pressure, the two of the results were adopted as examples for the numerical simulations. One is the uniaxial compressive test without lateral pressure by Barnard<sup>2)</sup>, and the other is the tri-axial compressive test by Hatanaka<sup>3)</sup>, et al.

First, Barnard's specimen is shown as Figure 2, and its dimensions are listed in Table 1. Figure 3 is an example of the obtained stress-strain relations.

Table 1 Dimensions of specimens

|                |                   |
|----------------|-------------------|
| height         | 11.5in. (29.21cm) |
| diameter(edge) | 4.5in. (11.43cm)  |
| ditto.(center) | 2.5in. ( 6.35cm)  |
| gauge length   | 4.0in. (10.16cm)  |

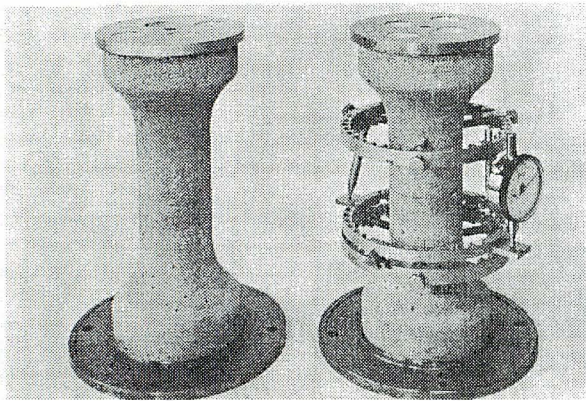


Fig. 2 Specimens<sup>2)</sup>

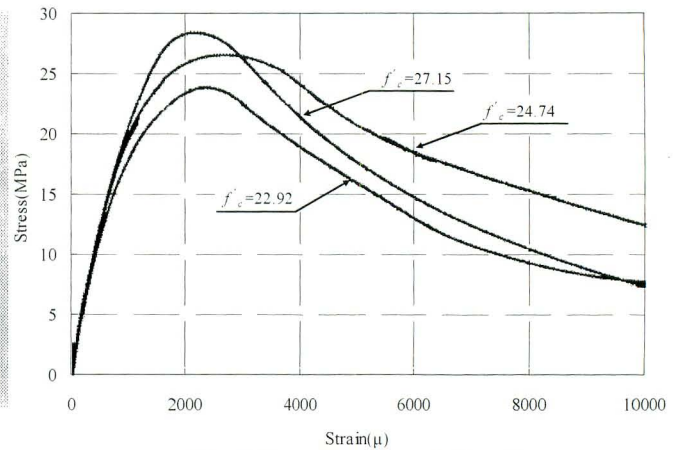


Fig. 3 Stress-strain relations<sup>2)</sup>

Next, Hatanaka's specimen and test setup is shown as Fig. 4, in which biaxial lateral pressure was given passively dependent on the lateral dilatation of the concrete specimen. Testing parameters and an example of the results are shown in Table 2 and Fig. 5, respectively.

Table 2 Outline of experiment<sup>3)</sup>

| water-cement ratio<br>W/C | height/width<br>H/D | Lateral confining stress $\sigma_L$<br>(MPa) |
|---------------------------|---------------------|--|
|                           |                     | 0  |
| 0.45                      | 1.0                 | 0.1  |
| 0.55                      | 1.3                 | 0.3  |
| 0.70                      | 2.0                 | 0.6 <sup>*1</sup>                            |
|                           |                     | 1.2 <sup>*2</sup>                            |

\*1:only for H/D=1

\*2:only for W/C=0.55 of H/D=1

average strain rate of  $2 \times 10^{-3}$ /min

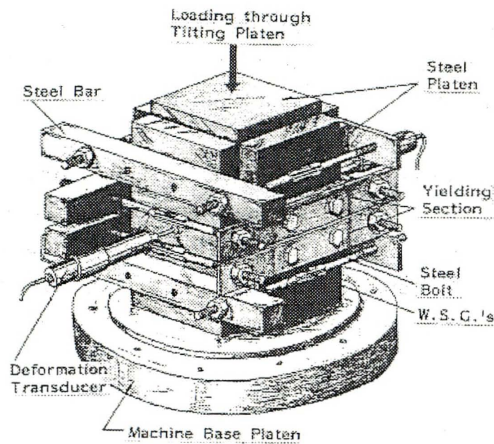


Fig. 4 Specimen and loading setup<sup>3)</sup>

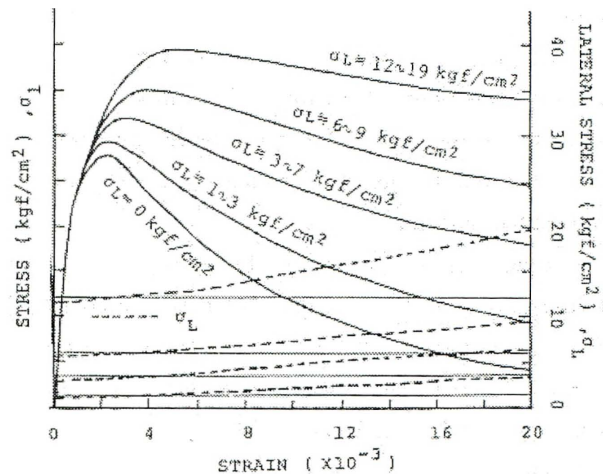


Fig. 5 Stress-strain relations<sup>3)</sup>

### 3. Elasto-Plastic Model for Strain-Softening

The determinations of loading conditions defined in stress space are given in Eqs.(1)-(3). Figures 6 and 7 show the conceptual two-dimensional views of the loading conditions of stress and strain spaces, respectively. When strain hardening and strain softening condition in the stress space are to be defined, it should be difficult to determine the condition of loading, neutral loading or unloading, because the determination equations, such as Eqs.(2) and (3), naturally involve multiple conditions.

$$df > 0 : \text{Loading (hardening)} \quad (1)$$

$$df < 0 : \text{Loading (softening), Unloading} \quad (2)$$

$$df = 0 : \text{Loading (perfect plasticity), Neutral loading} \quad (3)$$

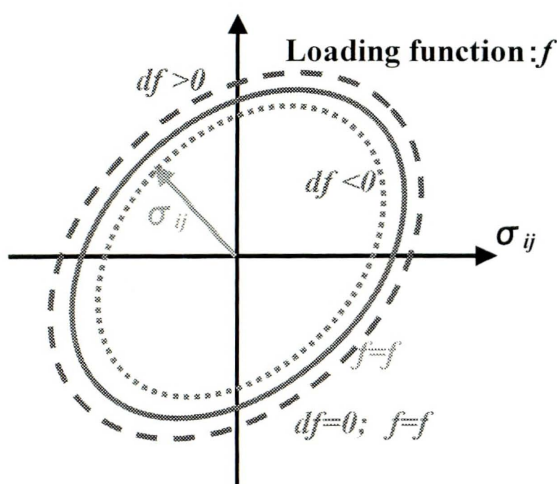


Fig. 6 Loading condition of stress space

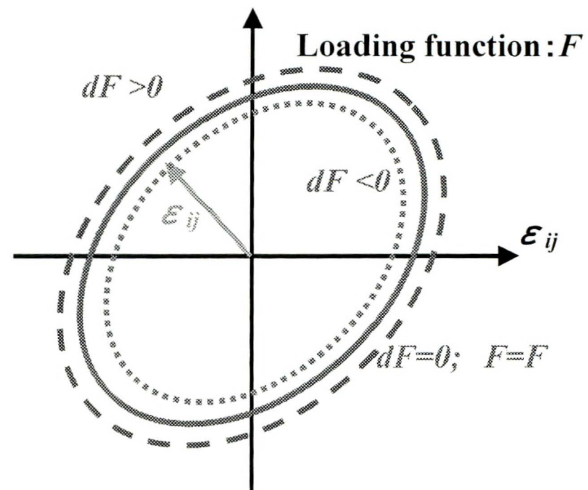


Fig. 7 Loading condition of strain space

The corresponding determination equations in strain space are also given in Eqs.(4)-(6). It can be found out that a consistent determination of the loading conditions is described without the above difficulty. Moreover, a comprehensive comparison of elasto plastic incremental theory between in stress and strain spaces is illustrated in Table 3.

$$dF > 0 : \text{Loading (hardening, softening, perfect plasticity)} \quad (4)$$

$$dF < 0 : \text{Unloading} \quad (5)$$

$$dF = 0 : \text{Neutral loading} \quad (6)$$

Table 3 Comparison between stress and strain space formulation

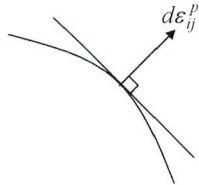
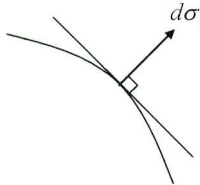
|                            | Stress space  | Strain space   |
|----------------------------|---|--|
| Loading function           | $f = f(\sigma_{ij}, \kappa) = 0$  | $F = F(\varepsilon_{ij}, \varepsilon_{ij}^p, \kappa) = 0$  |
| Flow rule                  | $d\varepsilon_{ij}^p = d\lambda \frac{\partial f}{\partial \sigma_{ij}}$ Drucker's postulate<br> | $d\sigma_{ij}^p = d\lambda \frac{\partial F}{\partial \varepsilon_{ij}}$ Il'yushin's postulate<br> |
| Stress-strain relationship | Compatibility condition<br>$df = \frac{\partial f}{\partial \sigma_{ij}} d\sigma_{ij} = 0$  | Compatibility condition<br>$dF = \frac{\partial F}{\partial \varepsilon_{ij}} d\varepsilon_{ij} = 0$   |

Figure 8 shows the loading function in three dimensional principal strain space. Equations (7) and (8)<sup>11</sup> are loading function:  $F$  and plastic potential function:  $G$ , respectively.

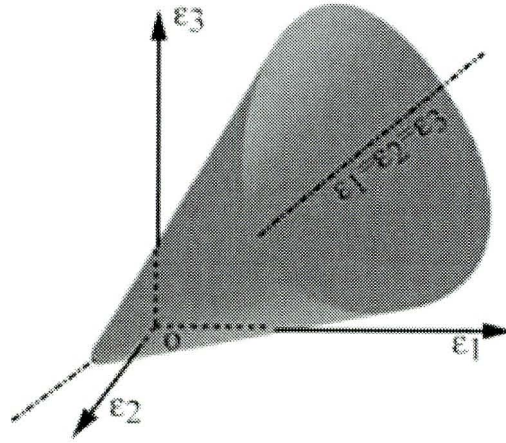


Fig.8 Loading function in a principal strain space

$$F = (\overline{AI_1} + a)^3 - \left[ 27 + f_p \left( \frac{P_a}{\overline{AI_1} + a} \right)^m \right] \left[ \frac{(\overline{AI_1} + a)^3}{27} - \frac{1}{3} (\overline{AI_1} + a) \overline{BJ_2} + \overline{CJ_3} \right] = 0 \quad (7)$$

$$G = (\overline{AI_1} + a)^3 - \left[ 27 + \eta_2 \left( \frac{P_a}{\overline{AI_1} + a} \right)^m \right] \left[ \frac{(\overline{AI_1} + a)^3}{27} - \frac{1}{3} (\overline{AI_1} + a) \overline{BJ_2} + \overline{CJ_3} \right] = 0 \quad (8)$$

where  $\bar{I}_1$ ,  $\bar{J}_2$  and  $\bar{J}_3$  = the first invariant of strain tensor and the second and third invariants of the deviatoric strain tensors, respectively;  $P_a$  = the atmospheric pressure;  $m$  = the shape parameter;  $a$  = a magnitude of movement to the tensile direction along the hydrostatic pressure axis; and  $f_p$  = the loading parameter. Moreover,  $\bar{A} = 3K$ ,  $\bar{B} = 4\mu^2$  and  $\bar{C} = 8\mu^3$ , where  $K$  and  $\mu$  are bulk and shear modulus, respectively.

Substituting by those into incremental stress-strain relation, the elasto plastic constitutive matrix in finite element formulation can be formed.

## 4. Numerical simulations

### 4.1 Preliminary

Compressive strength of concrete and also lateral confinement stress intensity are fundamentals for the behavior of the compressive concrete, so that their influences were examined preliminary.

First, the obtained results with the various compressive strengths are shown in Fig. 9. It could be found that the slope of the falling branch becomes steep as the given compressive strength is high, while the branches came together beyond the compressive strain of 10000 $\mu$  at last.

Next, Fig. 10 shows the results with the various confinements, in which the vertical axis indicates a normalized compressive stress by the corresponding compressive strength. From the results, the confinement intensity could considerably improve of the post-peak behavior, while it could not affect the peak stress.

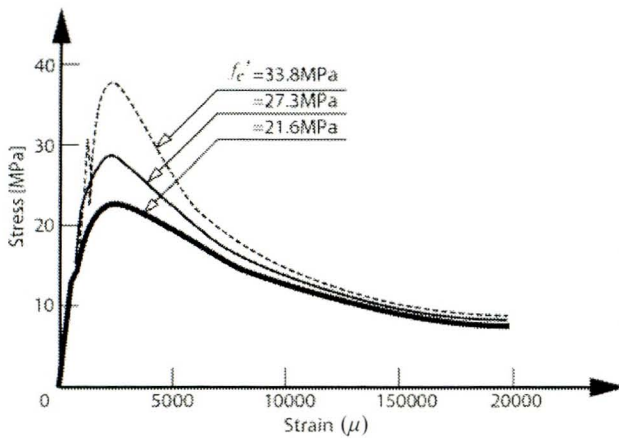


Fig. 9 Stress-strain relations with various compressive strengths

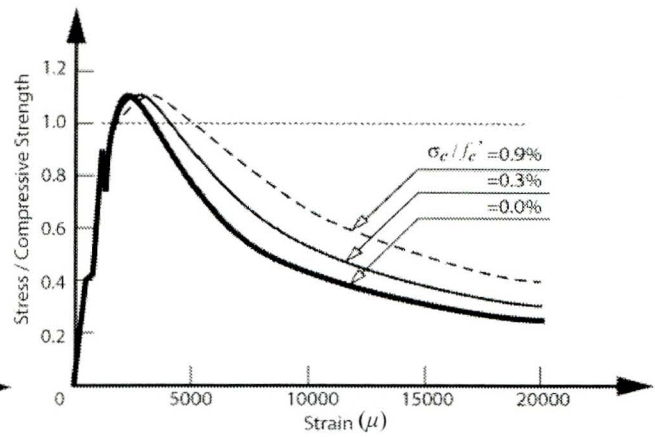


Fig. 10 Stress-strain relations with various confinement stresses

### 4.2 Material parameters

Material parameters of the material nonlinear model<sup>1)</sup> as described in the previous chapter 3 are listed in Table 4. It is noted that  $f_p$  relevant to  $\eta_1$  is the most essential to control the strain-softening behavior in the model. For example, the three of the parameters to be examined were  $\eta_1$ ,  $W_{ppeak}^0$  and  $\gamma_2$ , those are related closely to a uniaxial compression state. Figures 11, 12 and 13 are the results varying each of the corresponding three parameters, where each vertical axis denotes the normalized stress as same as that in Fig. 10. From these figures, it could be recognized in particular that the peak stress increased as  $\eta_1$  increases, as well as the post-peak branch arises as  $W_{ppeak}^0$  and  $\gamma_2$  increases.

Table 4 Material parameters of load function

|  |            |
|--|------------|
| $\eta_1$ :The peak value of parameter $f_p$  | 165        |
| $m$ :The shape parameter   | 0          |
| $a$ :A magnitude of movement to the tensile direction along the hydrostatic pressure | $0.31f'_c$ |
| $p$ :The value obtained by using least square method                                 | 0.099      |
| $l$ :The value obtained by using least square method                                 | 0.867      |
| $W^0_{ppeak}$ :The plastic work corresponding to the non lateral pressure            | 0.345      |
| $\gamma_1$ :The value obtained by using least square method                          | 0.1021     |
| $\gamma_2$ :The value obtained by using least square method                          | 2.41       |

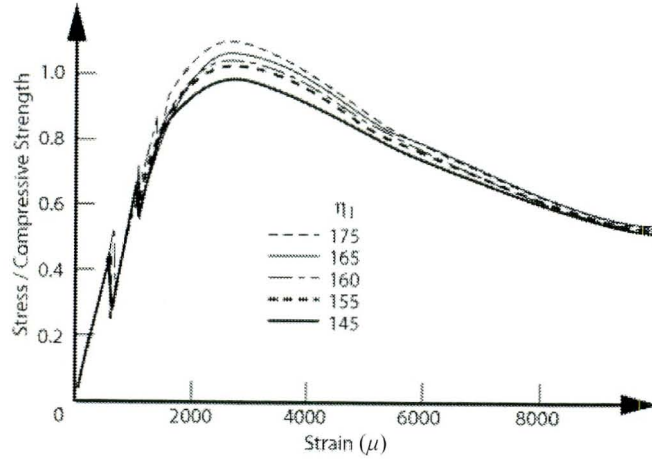


Fig.11 Stress-strain relations with various  $\eta_1$

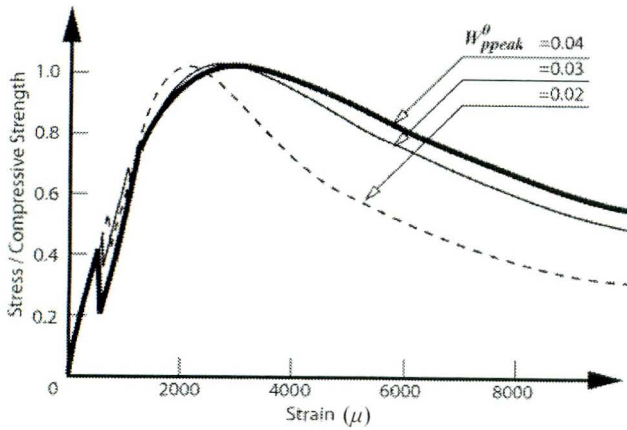


Fig.12 Stress-strain relations with various  $W^0_{ppeak}$

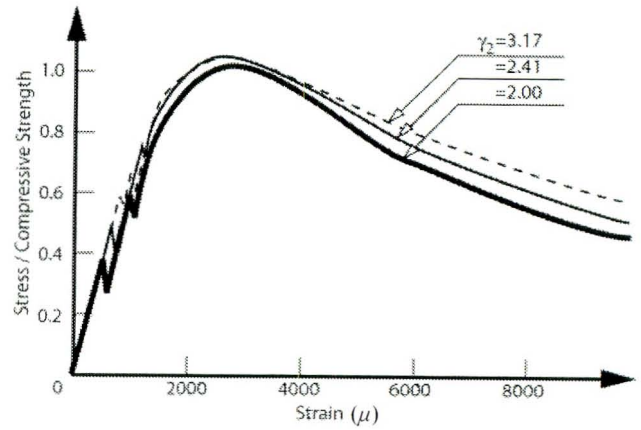


Fig.13 Stress-strain relations with various  $\gamma_2$

### 4.3 Application to existing results

The numerical simulations based on the material nonlinear modeling were conducted on two of the existing experimental evidences as introduced in the chapter2. One was under uniaxial compression only, and the other was under the compression with lateral confinement pressure, so-called triaxial compression.

First, the results for the former under uniaxial compression are shown in Fig.14, in which the values of the material parameters in Table 4 were used. Because the parameters were adjusted for another concrete material from Ref.2), there were naturally some differences between the experimental and numerical curves. Thus, another simulation have been carried out, modifying the set of the parameters as  $\eta_1 = 155$ ,  $W_{peak}^0 = 0.02$  and  $\gamma_2 = 2.41$ . As the modified results, better agreements could be obtained as shown in Fig.15, although slight differences on the peak stresses were hold.

Next, the results for the latter under triaxial compression are shown in Fig.16. Comparing the experimental and numerical results, a satisfactory agreement of the peak stress point could be obtained, although a slight leftward sift of the point appeared for the case with the highest lateral pressure. Furthermore, as to the post-peak branch, the numerical results could trace well along the corresponding experimental ones, except for the case of no lateral pressure.

Consequently, the numerical modeling discussed here could be effective to evaluate the post-peak behavior of compressive concrete with lateral confinement stress.

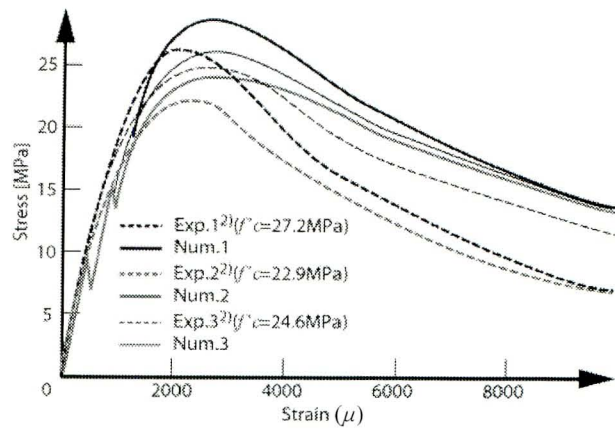


Fig.14 Stress-strain relations according to the parameter values in Table 4

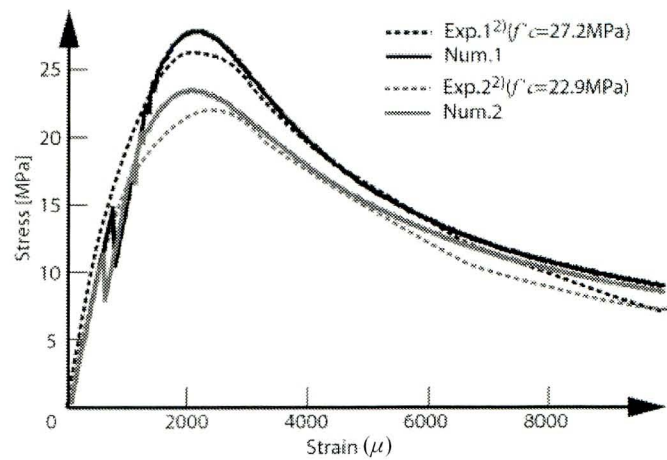


Fig.15 Stress-strain relations using modified parameter values

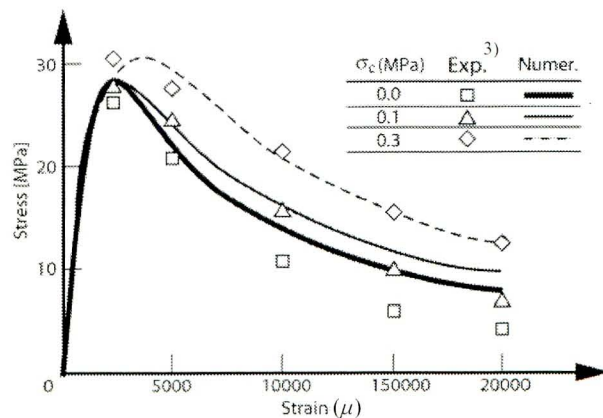


Fig.16 stress-strain relations with various lateral confinement stresses

## **5. Concluding Remarks**

From the parametric studies on compressive concrete as a strain softening material, the followings are concluded.

- (1) Essential material parameters for the load function were obtained.
- (2) Satisfactory solutions have been obtained for the existing experimental results.
- (3) Confinement effect can be also evaluated including post-peak region.

## **6. References**

- 1) Mizino and Hatanaka: Compressive softening model for concrete, Journal of Engineering Mechanics, ASCE, Vol.118, No.8, pp.1546-1563, (1992)
- 2) P. R. Barnard: Researches into the complete stress-strain curve for concrete, Magazine of Concrete Research, Vol.16, No.49, pp.203-210, (1964)
- 3) Hatanaka, S., Kosaka, Y. and Tanigawa, Y.; Plastic deformational behavior of axially loaded concrete under low lateral pressure -An evaluation method for compressive toughness of laterally confined concretes (part 1), Transactions of AIJ, No.377, pp.27-40, (1987)